

MULTI-POLARIZATION DIMENSIONALITY OF MULTI-ANTENNA SYSTEMS

M. S. Elnaggar

CALIT2

University of California San Diego
9500 Gilman Drive, La Jolla, CA 92093-0436, USA

S. K. Chaudhuri and S. Safavi-Naeini

ECE Department

University of Waterloo
200 University Ave W, Waterloo, ON, N2L 3G1, Canada

Abstract—Based on the deterministic Maxwellian framework, we investigate the ability of each of the dual fields (electric and magnetic) in carrying independent information in a multi-polarization MIMO system. We quantify the performance by using a well-defined power independent dimensionality (PID) metric. We present numerical results for 3 deterministic scenarios: a canonical free-space (near and far field exact solution), a canonical PEC corridor (using rigorous modal analysis) and a lossy-wall corridor (using image ray tracing). The deterministic results show that in a multi-path rich environment, the hexapole system (collocated polarized electric and magnetic point radiators) is almost guaranteed to provide more than 3 DOF. However, in the simulated scenarios, the maximum 6 DOF are never attained due to the inevitable coupling between the electric and magnetic fields. On the other hand, for a tripole system, the upper-limit of 3 DOF is achievable.

1. INTRODUCTION

In this paper, we deterministically investigate the degree of freedom (DOF) gain (i.e., creation of new parallel channels) which can be provided through a collocated multi-polarization MIMO system. “Multi-polarization” designates transmit/receive collocated configurations, namely, tripoles (3 mutually-orthogonal collocated

Corresponding author: M. S. Elnaggar (michel@ucsd.edu).

point sources forming 3 independent ports), hexapoles (2 collocated dual tripoles i.e., electric and magnetic as described in [1, 2]), or other combined dual polarization cases.

The problem addressed in this work is eventually a single-point sampling (through infinitesimal electric/magnetic dipoles) of a vector-field which happens to experience 2 types of collocated spatial orthogonality: *vectorial* and (scalar) *functional* [2]. The former is the essence of the polarization diversity whereas one form of the latter is the pattern diversity in the *far-field* modeling.

Various deterministic simulations in this work show that the vectorial and functional orthogonality are not necessarily independent due to the inevitable coupling between the electric and magnetic field components. Consequently, the claim of hexapole six-fold dimensionality gain [1, 2] under statistical channel assumption is not practically guaranteed. Certainly, the results of the deterministic simulations performed in this work cannot be strictly generalized to *every* environment or even to a class of environments as is the case with the stochastic case. Nevertheless, such deterministic simulations accurately account (in the Maxwellian sense [5, 6]) for the coupling between the electric and magnetic fields, a feature which is overlooked in the statistical approach. We thus claim that the novelty of this work is the application of accurate deterministic techniques to draw some conclusions regarding the dimensionality of multi-polarized MIMO systems in the given environments.

We attempt to provide a clear answer to the following controversial question raised in the literature [1–4]: can each of the electric and magnetic fields carry an independent piece of information between 2 radiating structures and thus double the one-field communication dimensions? The challenge in this question lies in the fact that the 2 fields are not simultaneously arbitrary since they are related by Maxwell’s equations. Through a universal model sustained by numerical results, we show that the answer depends on the 2 intertwined orthogonality types, which are environment-specific.

We begin by setting a generic framework for multi-polarization scenarios by using a 6×6 polarization matrix based on Maxwell’s equations. A canonical free-space (near and far field) scenario is then thoroughly investigated showing a particular transmit/receive separation at which full-rank dimensionality is achievable using tripoles. Next, we show multi-polarization results in a corridor having perfect electric conductor (PEC) walls by using rigorous modal analysis. Afterward, we repeat the corridor simulation, through approximate image ray tracing (IRT), in another scenario when the walls are “transparent” i.e., having a small loss-tangent

(LT). We conclude by showing a histogram of the multi-polarization dimensionality results of the simulated scenarios.

2. UNIVERSAL MULTI-POLARIZATION MODELING

In order to isolate the multi-polarization effect, we deliberately exclude the space diversity by employing collocated infinitesimal (Hertzian) dipoles as a perfect multi-polarization “field-probe”, having a zero-length and detecting the vectorial nature of the electromagnetic fields. Nevertheless, we must admit that the polarization diversity is inseparable of the pattern diversity, which ultimately makes the multi-polarization zero-length MIMO system founded on the combined pattern/polarization diversity. In fact, this double-diversity is the base of the 2 aforementioned types of collocated spatial orthogonality (vectorial and functional).

Similarly to [2], we employ the polarization matrix $\mathbf{H}_6 \in \mathbb{C}^{6 \times 6}$, which models the 6×6 MIMO channel between the transmit/receive hexapoles. For m or $n = \{1, 2, 3\}$, the element h_{mn} represents an *electrical* receive/transmit, where (1, 2, 3) denote indices for the 3 mutually orthogonal coordinates. Similarly, for m or $n = \{4, 5, 6\}$, h_{mn} represents a *magnetic* receive/transmit, where (4, 5, 6) denote indices for the same 3 mutually orthogonal coordinates, respectively. We assume narrow-band operation of the system. Moreover, the following source normalization assumptions are made:

1. The electric (I_{El}) and magnetic (I_{Ml}) dipole moments are normalized such that $(I_{Ml}) = \eta_0(I_{El})$, where $\eta_0 = 120\pi$ is the free-space impedance.
2. The received signal, either by an electric or magnetic infinitesimal dipole, is detected as a proportional voltage. Therefore, any receive magnetic field component is multiplied by η_0 in the following analysis.

From the duality between the electric and magnetic fields [7], the hexapole channel matrix \mathbf{H}_6 is expressed as

$$\mathbf{H}_6 = \begin{pmatrix} \mathbf{C} & -\mathbf{D} \\ \mathbf{D} & \mathbf{C} \end{pmatrix}, \quad (1)$$

where, for $n = \{1, 2, 3\}$, the column vectors c_n and d_n of the 3×3 sub-matrices \mathbf{C} and \mathbf{D} represent the receive electric and magnetic fields response, respectively, to the n th polarized transmit *electrical* excitation. Furthermore, at the receive point, the source-free Maxwell's

curl equations must be satisfied

$$\nabla \times \overline{\mathbf{E}} = -j\omega\mu_0\overline{\mathbf{H}} \quad (2a)$$

$$\nabla \times \overline{\mathbf{H}} = j\omega\varepsilon_0\overline{\mathbf{E}}. \quad (2b)$$

Therefore, from the aforementioned source-normalization assumptions and (2a), the sub-matrices \mathbf{C} and \mathbf{D} are related by

$$\mathbf{D} = \eta_0 \frac{\overline{\nabla} \times \mathbf{C}}{-j\omega\mu_0} = \frac{j}{k_0} \overline{\nabla} \times \mathbf{C}, \quad (3)$$

where $\overline{\nabla} \times \mathbf{C}$ is a dyadic curl (operating on the column vectors of \mathbf{C}) and k_0 is the free space wave number. Accordingly, \mathbf{H}_6 is expressed as

$$\mathbf{H}_6 = \begin{pmatrix} \mathbf{C} & -\frac{j}{k_0} \overline{\nabla} \times \mathbf{C} \\ \frac{j}{k_0} \overline{\nabla} \times \mathbf{C} & \mathbf{C} \end{pmatrix}. \quad (4)$$

Equation (4) is *universal* at any *source-free* point in any environment as long as we are operating the system in narrow-band and the environment electrical/magnetic properties are deterministic at any one time. At any point in space where there is an impressed source or medium inhomogeneity (e.g., at the boundaries), (4) is not true.

Now, we return back to the question regarding the usage of $\overline{\mathbf{E}}$ and $\overline{\mathbf{H}}$ as independent information carriers. From (4), given the fact that the elements of \mathbf{H}_6 are not all independent, can we really achieve 6 DOF? The answer was positive in [1, 2] and negative in [3, 4]. The deterministic results of this work provide evidence that by employing a hexapole system, we *can* have more than 3 DOF *if* the environment permits. However, in all these deterministic simulations, the maximum 6 DOF have not been attained.

Hence, the core of the answer is how to exploit the 2 orthogonality types in the *deterministic environment* as modeled by \mathbf{H}_6 . The matrix rank becomes deficient when there exists a *linear algebraic* dependence between the matrix rows or columns. In (4), there is a linear dependence, however, it is *differential* rather than algebraic and has therefore no clear impact on the matrix rank. The environment properties, manifested through the boundary conditions, set the explicit *algebraic* dependence between \mathbf{C} and \mathbf{D} in (1). We will see in the upcoming case studies that whenever this differential dependence approximates a linear algebraic one (single plane-wave or spherical ray), only then, the rank becomes deficient.

The vectorial orthogonality is exhibited through the 3 components of one vector field (either electric $\overline{\mathbf{E}}$ or magnetic $\overline{\mathbf{H}}$ but not both)

along the 3 mutually orthogonal coordinates. Hence, the vectorial orthogonality is also known as the polarization diversity. If the dual fields (\overline{E} and \overline{H}) were independent (uncoupled), a pair of infinitesimal dual tripoles (electric and magnetic) would be sufficient to allow up to 6 DOF through independent vectorial orthogonality. However, the dual fields are indeed coupled; otherwise, the *electromagnetic* propagation would not exist. Therefore, in order to employ the DOF of the dual field, it is mandatory to have another sort of diversity, which is accomplished through the so-called Field Expansion Diversity (FED). The FED is also known as the functional orthogonality or, in the far-field analysis, pattern diversity. The terms functional orthogonality and FED are used interchangeably hereafter.

The FED is best understood when the received field is expressed as an integration (or summation in discrete analysis) of some field expansion components such as:

- The spherical propagating multipath rays in the case of high-frequency approximation (ray tracing). We emphasize that in this case, each ray should be considered inseparably of the transmit/receive pattern-weighting [2].
- In general, the plane-wave expansion components of the received field [8].
- The modes in a PEC waveguide, which can straightforwardly be further decomposed into a summation of plane waves.

At a given angular direction, an expansion component is individually rank-deficient of rank 2 [4]. Nevertheless, the integration (summation) of all the expansion components *can* produce a resultant higher rank matrix of better DOF [1, 2]. Consequently, a rank-deficient expansion component is not automatically a bottle-neck for the DOF of the multi-polarization MIMO system as was argued in [4]. In case of ray modeling, such FED is traditionally known as the antenna far-field *pattern diversity* [2] since the weighted-integration (summation) of the multipath rays is done through the antenna patterns over the visible angular domain.

Within each plane-wave or spherical ray component, there is a linear algebraic dependence between the transverse electric and magnetic field components meaning that only one field can carry independent information. By only considering the independent electric field in each plane wave component, we have the following double-impact when *all* the plane-wave components impinge on a hexapole receive from *different directions*:

- Even though each plane wave individually allows 2 DOF based on partial vectorial orthogonality (the 2 transverse components of

the electric field), the plane-wave integration/summation creates a third vectorial electric DOF because the resultant electric field now has 3 components [1].

- Each field component (say E_z) of an impinging plane wave has the potential to interact with 3 receive elements (*electric z-polarized* and *transverse magnetic x- and y-polarized* elements). However, these 3 receive elements interpret differently the same field component according to the plane-wave direction of arrival. Ultimately, when *all* the plane waves are angularly weighted (integration/summation), such functional orthogonality gives room to more DOF [2].

Therefore, in the hexapole system, we are exploiting the vectorial nature of *one field* along with the angular sensitivity of the *dual-field detector* (rather than the dual-field itself, which is not independent) to convey independent information. Accordingly, the aforementioned question becomes whether the same mechanism (plane-wave expansion) can provide 2 independent orthogonality effects. The numerical results obtained in this work show that there is an inevitable coupling between these 2 orthogonality effects.

3. A CANONICAL FREE-SPACE MULTI-POLARIZATION SCENARIO

In this section, we investigate the dependence of the multi-polarized MIMO system DOF on the transmit/receive separation in free-space (near and far field). We employ a recently developed power-independent dimensionality (PID) metric [11] for the purpose of DOF evaluation throughout this paper. The PID definition and relevant properties are briefly stated in Appendix A. The justification of such a power-independent perspective in MIMO dimensionality evaluation is also discussed in Appendix A.

For a z -polarized infinitesimal electrical dipole in free space, the *exact* closed-form expressions of the field components in spherical

coordinates are given by [9]

$$\begin{aligned}
 E_r &= (I_{El}) \eta_0 \frac{\cos \theta}{2\pi r^2} \left(1 + \frac{1}{jk_0 r}\right) e^{-jk_0 r} \\
 E_\theta &= j (I_{El}) \eta_0 \frac{k_0 \sin \theta}{4\pi r} \left(1 + \frac{1}{jk_0 r} - \frac{1}{(k_0 r)^2}\right) e^{-jk_0 r} \\
 H_\varphi &= j (I_{El}) \frac{k_0 \sin \theta}{4\pi r} \left(1 + \frac{1}{jk_0 r}\right) e^{-jk_0 r} \\
 E_\varphi &= H_r = H_\theta = 0
 \end{aligned} \tag{5}$$

By duality, for a z -polarized infinitesimal magnetic dipole in free space, the field components are given by [9]

$$\begin{aligned}
 H_r &= \frac{(I_M l)}{\eta_0} \frac{\cos \theta}{2\pi r^2} \left(1 + \frac{1}{jk_0 r}\right) e^{-jk_0 r} \\
 H_\theta &= j \frac{(I_M l)}{\eta_0} \frac{k_0 \sin \theta}{4\pi r} \left(1 + \frac{1}{jk_0 r} - \frac{1}{(k_0 r)^2}\right) e^{-jk_0 r} \\
 E_\varphi &= -j (I_M l) \frac{k_0 \sin \theta}{4\pi r} \left(1 + \frac{1}{jk_0 r}\right) e^{-jk_0 r} \\
 E_r &= E_\theta = H_\varphi = 0
 \end{aligned} \tag{6}$$

We begin by constructing the hexapole matrix and we follow the normalization assumptions of Section 2. We also assume an orientation as depicted in Fig. 1 for the transmit/receive hexapoles (2 broadside/1 endfire setup) and the hexapoles are separated by a distance r . Any arbitrary transmit/receive rotation is modeled by a unitary matrix with has no effect on the singular values of the channel matrix. This is true as well for other general scenarios.

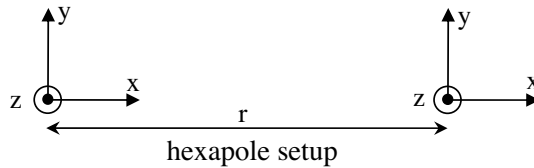


Figure 1. Each end (transmit/receive) accommodates 2 collocated dual tripoles each consisting of 2 broadside and 1 endfire elements.

We choose the Cartesian coordinates to construct \mathbf{H}_6 such that the indices (1, 2, 3) of the elements h_{mn} denote the (x, y, z) coordinates for *electrical* receive/transmit whereas the indices (4, 5, 6)

of the elements h_{mn} denote the (x, y, z) coordinates for *magnetic* receive/transmit. According to Fig. 1, using (5) and (6) along with coordinate transformation and the aforementioned normalization assumptions, \mathbf{H}_6 is constructed yielding

$$\mathbf{H}_6 = \begin{bmatrix} a_1 & 0 & 0 & 0 & 0 & 0 \\ 0 & a_2 & 0 & 0 & 0 & a_3 \\ 0 & 0 & a_2 & 0 & -a_3 & 0 \\ 0 & 0 & 0 & a_1 & 0 & 0 \\ 0 & 0 & -a_3 & 0 & a_2 & 0 \\ 0 & a_3 & 0 & 0 & 0 & a_2 \end{bmatrix}, \quad (7a)$$

where, after multiplying the field components by $4\pi r^2$ and omitting the common factors,

$$\begin{aligned} a_1 &= 2(1 + \xi^{-1}) \\ a_2 &= \xi + 1 + \xi^{-1} \\ a_3 &= \xi + 1 \\ \xi &= jk_0 r \end{aligned}. \quad (7b)$$

Consequently, the singular values of \mathbf{H}_6 are obtained from (7) yielding

$$\sigma\{\mathbf{H}_6\} = \{|a_1|, |a_1|, |a_2 + a_3|, |a_2 + a_3|, |a_2 - a_3|, |a_2 - a_3|\}, \quad (8)$$

where each singular value has a multiplicity of 2 [2].

In a similar fashion, we can extract from the generic \mathbf{H}_6 other multi-polarization systems:

- the 3×3 tripole matrix \mathbf{H}_3 .
- the 4×4 tetrapole matrices \mathbf{H}_{3e} and \mathbf{H}_{3b} consisting of (1 tripole, 1 dual endfire) and (1 tripole, 1 dual broadside) polarizations, respectively.
- the 5×5 pentapole matrices \mathbf{H}_{3eb} and \mathbf{H}_{3bb} consisting of (1 tripole, 1 dual endfire, 1 dual broadside) and (1 tripole, 2 dual broadside) polarizations, respectively.

Table 1 includes the closed-form singular values as well as the near-field ($a_1/a_2 \rightarrow 2$ and $a_3/a_2 \rightarrow 0$) and far-field ($a_1/a_2 \rightarrow 0$ and $a_3/a_2 \rightarrow 1$) PID values. Fig. 2 depicts the distance-dependence of the PID for the multi-polarization scenarios.

The PID of case 1 and 2 in Table 1 reaches its maximum, rank (\mathbf{H}), at one specific separation when $|a_1| = |a_2|$, which occurs at

$$\frac{r}{\lambda} = \frac{1}{2\pi} \sqrt{\frac{5 + \sqrt{37}}{2}} \approx 0.3747, \quad (9)$$

Table 1. Summary of multi-polarization results.

Pol. Case	Singular Values	Near-Field PID $k_0 r \ll 1$	Far-Field PID $k_0 r \gg 1$
1 Tripole	$\sigma\{\mathbf{H}_3\} = \{ a_1 , a_2 \}$	$8/3 \approx 2.67$	2
2 Tripole 1 endfire	$\sigma\{\mathbf{H}_{3e}\} = \{ a_1 , a_2 \}$	3.6	2
3 Tripole 1 broadside	$\sigma\{\mathbf{H}_{3b}\} = \{ a_1 , a_2 + a_3 , a_2 - a_3 \}$	$25/7 \approx 3.57$	1.8
4 Tripole 1 endfire 1 broadside	$\sigma\{\mathbf{H}_{3eb}\} = \{ a_1 , a_2 + a_3 , a_2 - a_3 \}$	$49/11 \approx 4.45$	1.8
5 Tripole 2 broadside	$\sigma\{\mathbf{H}_{3bb}\}$ $= \{ a_1 , a_2 + a_3 , a_2 - a_3 \}$	4.5	2
6 Hexapole	$\sigma\{\mathbf{H}_6\}$ $= \{ a_1 , a_2 + a_3 , a_2 - a_3 \}$	$16/3 \approx 5.33$	2

where λ is the free space wavelength. For all the other cases, the inevitable coupling between the electric and magnetic field prevents the PID from reaching rank (\mathbf{H}) and the maximum PID occurs in the near-field region ($k_0 r \ll 1$).

In the far-field analysis, the spherical wave approaches a single traveling plane-wave (within a vicinity of some transmit/receive separation r to disregard the $1/r$ decay of the field). Therefore, the far-field scenario lacks any FED orthogonality since there is only one “plane-wave” component. Moreover, the absence of any field radial component reduces the vectorial orthogonality to 2. Consequently, we get the well-known horizontal and vertical polarization diversity for the hexapole system in the far-field region. From a matrix-modeling perspective, the far-field scenario approaches a matrix of rank 2, given the fact that there is a *linear algebraic* dependence between the transverse component of \overline{E} and \overline{H} . For case 3 and 4 in Table 1, the 2 channels have non-equal contributions $\{2|a_2|, |a_2|\}$. Therefore, from a dimensionality perspective, case 3 and 4 dimensionality performance is less than 2.

On the other hand, the near-field analysis of this canonical free-space scenario is more enlightening. The rigorously derived results shed light on possible near-field applications such as short-distance/low-frequency indoor MIMO systems based on collocated

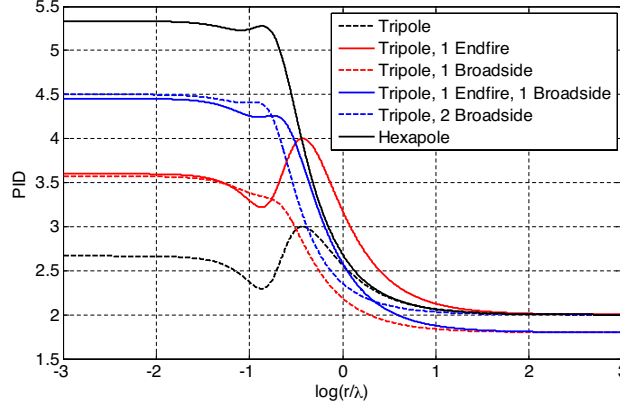


Figure 2. PID vs r/λ (log-scale) for free-space multi-polarization scenarios.

multi-polarization. We use the plane-wave expansion of the spherical wave [8] to show that this near-field scenario, which seemingly has no multipath richness, is indeed *super-rich*. We assume a propagation hemisphere cross-section at $z = 0$ (the chosen decay direction of the evanescent components is along the positive z -axis). Comparing the field vector potential analysis to the plane-wave expansion of the field of an electrical point source, we get [8]

$$\frac{e^{-jk_0 r}}{r} = \frac{1}{j2\pi} \int_{-\infty}^{\infty} \int_{-\infty}^{\infty} \frac{e^{-jk_0 \hat{k} \cdot \bar{r}}}{k_z} dk_x dk_y, \quad (10)$$

where $\bar{r} = (x, y, z)$ is the position vector of the observation point with respect to the point source and $\hat{k} = \frac{1}{k_0}(k_x, k_y, k_z)$ is a *complex* unit vector ($\hat{k} \cdot \hat{k} = 1$). According to our choice of the hemisphere cross-section at $z = 0$, k_x and k_y are always real (spanning the extended visible and evanescent angular domain). Accordingly, k_z is either real or pure imaginary as follows:

- For $k_x^2 + k_y^2 < k_0^2$, $k_z = +\sqrt{k_0^2 - k_x^2 - k_y^2}$ (positive real) and \hat{k} is the propagation direction of the traveling plane wave component.
- For $k_x^2 + k_y^2 > k_0^2$, $k_z = -j\sqrt{k_x^2 + k_y^2 - k_0^2}$ (negative pure imaginary) and the evanescent plane wave component is decaying in the positive z -direction at a rate of $e^{-|k_z|z}$.

Because of the closed-form in the left-hand side of (10), we were able to exactly derive the field solution (5) and (6) in closed-form through Maxwell's equations, and the solution includes *all* the evanescent waves components, which is not computationally available in the bounded electromagnetic problems. In the extended angular domain, the spectrum of (5) and (6) exhibits an *ultra-wide spatial bandwidth* (traveling and evanescent). In other words, the near-field analysis of a free-space scenario resembles a *super-rich* multipath environment (including traveling and evanescent waves). Although each plane-wave (traveling or evanescent) has individually 2 DOF, the integration of all plane-wave components yields a higher DOF, which is against the argument of [4] concerning the strict upper limit of 2 DOF for the multi-polarization systems. Both the FED orthogonality and the existence of a radial field component (full vectorial orthogonality) contribute to this higher DOF. However, the coupling between the electric and magnetic fields does not allow the PID to reach the full-rank value of 6.

The multi-polarization near-field DOF results in this example gives an idea about the *expected* DOF in a realistic multipath scenario: if a super-rich near-field environment does not achieve 6 DOF as already shown by rigorous analysis, it seems *likely* that most other environments may not achieve 6 DOF either. The results of the next section agree with this expectation.

4. MULTI-POLARIZATION IN A PEC CORRIDOR SCENARIO: MODAL ANALYSIS

We move now to investigate the multi-polarization DOF in a canonical indoor scenario. The environment is a rectangular open-ended corridor (waveguide) having PEC walls. Such a canonical structure is highly multipath-rich. We employ the modal field solution for this multi-polarization excitation under the PEC boundary conditions. The corridor width and height are 4 m and 3 m, respectively. The operating frequency is 2.4123 GHz, so chosen to avoid numerical complexity in the modal solution. Under these operating conditions (frequency and corridor dimensions), we have 2495 propagating modes.

As shown in Fig. 3, we denote the axis along the corridor length, width and height by (L, W, H) , respectively. The multi-polarized transmit is located at $(2, 2.8)$ along (W, H) , respectively. The multi-polarized receive is moving over a grid of equidistant 100×100 points on the whole cross-section of the corridor. The simulation is repeated over 3 grids situated at 25, 30 and 40 m from the transmit point along the L -axis. Such distances are sufficient to guarantee the suppression

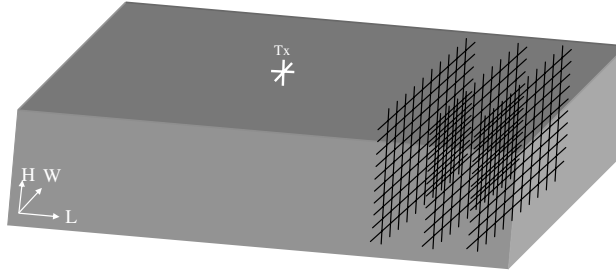


Figure 3. Multi-polarization scenarios in a corridor.

of all the evanescent modes.

In the 3 simulated scenarios, we obtained very similar PID results. The average value for the PID for the tripoles and hexapoles systems over the grid locations is 2.35 and 4.3, respectively. An example of the PID over the grid points at 30 m L -separation is shown in Fig. 4. Very close average values were obtained as well when the transmit and grid points were re-located to other positions.

We can make several interesting observations from Fig. 4. In the hexapole case, 3 DOF or more are almost guaranteed. However, as expected earlier from the near-field free-space scenario, the full-rank 6 DOF have never been achieved in this rigorously-modeled multipath-rich environment. The reason for having less than full 6 DOF is attributed to the coupling between the electric and magnetic fields, which impacts the independence between the vectorial and functional orthogonality.

For the tripole scenario, the full-rank 3 DOF can be closely approached. Nevertheless, there are few occurrences of $\text{PID} < 2$. In spite of the 2 DOF of each plane-wave component, their summation may accidentally yield lower dimensionality. This observation can be explained by a destructive interference that suppresses one out of the available 3 components of the electric field while there is a discrepancy in the values of the other 2 components (similar to case 3 and 4 in Table 1). In the hexapole case, such a suppression of 3 or more out of the 6 components of the electric and magnetic fields is very unlikely.

5. MULTI-POLARIZATION IN A TRANSPARENT-WALL CORRIDOR SCENARIO: IRT SIMULATION

The multi-polarization DOF gain is now investigated in a more practical indoor scenario. The environment is a rectangular corridor of dimensions $100 \times 4 \times 3$ m along (L, W, H) , respectively. The walls

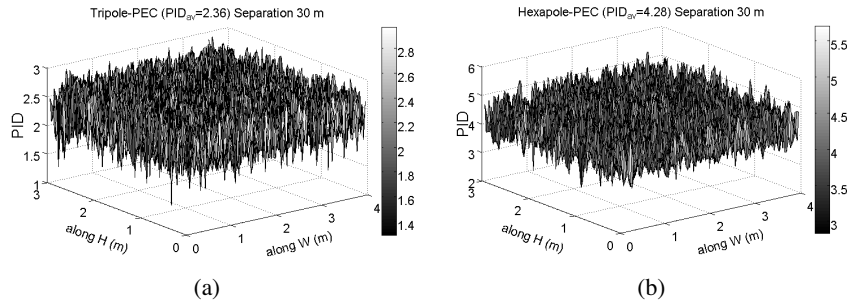


Figure 4. PID of multi-polarization MIMO system in a PEC corridor. The receive grid is located at 30 m from the transmit along L . (a) Tripole. (b) Hexapole.

thickness is 15 cm with a dielectric constant of 4 and a LT of 0.02. The ceiling and floor thicknesses are 30 cm with a dielectric constant of 6 and a LT of 0.05. We set up comparable scenarios to the PEC corridor in Section 4. The multi-polarized transmit is located at (50, 2, 2.8) along (L , W , H), respectively. The operating frequency is also 2.4123 GHz. The multi-polarized receive is moving over a grid of equidistant 20×20 points on the whole cross-section of the corridor. The simulation is repeated over 3 receive grids situated at 75, 80, 90 m along the L -axis as sketched in Fig. 3.

Such a transparent-wall corridor is a LOS environment and does not enjoy the same multipath richness as the PEC counterpart. We employ a 3D-IRT algorithm to evaluate the channel matrix at each receive grid point. The entries of \mathbf{H}_6 are constructed by applying the spherical ray expansion such that

$$h_{mn} = \sum_{l=1}^{\infty} \mathbf{e}_{ml}^{(r)T} \cdot \bar{\mathbf{D}}_l^{(rt)} \cdot \mathbf{e}_{nl}^{(t)} \frac{\exp(-jk_0 R_l)}{R_l}, \quad (11)$$

where the index l represents the ray order; $\mathbf{e}_{nl}^{(t)}$ and $\mathbf{e}_{ml}^{(r)}$ are the transmit/receive far *electric* field pattern/polarization vector (effective length) at the proper ray departure/arrival direction, respectively, each having 2 components in θ and φ directions; and $\bar{\mathbf{D}}_l^{(rt)}$ is the far-field environment ray-dyad (2×2), which models the reflection loss and the polarization rotation along the l th ray path and excludes the free space spherical propagation factor $\exp(-jk_0 R_l)/R_l$. Since the 6 multipole elements are located at the same physical location, we omit the subscripts m , n from the dyad $\bar{\mathbf{D}}_l^{(rt)}$, which depends only on the ray departure/arrival angles, and the environment geometrical/electrical

properties.

In order to readily obtain the far-field pattern/polarization (*electric* effective length) of a point *electric current* source, polarized in the $\hat{\mathbf{a}}_\xi$ direction, we use the following decomposition

$$\mathbf{e} = -(\hat{\mathbf{a}}_\xi \cdot \hat{\mathbf{a}}_\theta) \hat{\mathbf{a}}_\theta - (\hat{\mathbf{a}}_\xi \cdot \hat{\mathbf{a}}_\varphi) \hat{\mathbf{a}}_\varphi. \quad (12)$$

Then, to get the *electric* effective length of a point *magnetic current* source, we apply the duality principle.

Since there is a linear algebraic dependence between the transverse components of the magnetic and electric field along each ray, the multipole PID *per ray* can never exceed 2 (the vectorial orthogonality of one-field) and thus the IRT simulator needs to trace the *electric field* only. However, the summation (11) introduces a third vectorial DOF [1] as well as the functional orthogonality due to the pattern orthogonal weighting (pattern diversity or FED), which is modeled by $\mathbf{e}_{nl}^{(t)}$ and $\mathbf{e}_{ml}^{(r)}$.

In [10], we found out that few hundred rays are sufficient to yield a convergent solution in the case of transparent walls (small LT). We employ in the simulations herein the most significant 1000 rays, which are traced from the fixed multi-polarization transmit to the moving multi-polarization receive at each grid point. Fig. 5 show the PID over the grid locations at a separation 30 m along L by using tripoles and hexapoles. The PID results are very similar in the other scenarios and the average PID is 1.9 and 2.4 for the tripole and hexapole systems, respectively. The lack of multipath-richness due to the transparent (lossy) walls has significantly reduced the DOF in comparison with the PEC corridor.

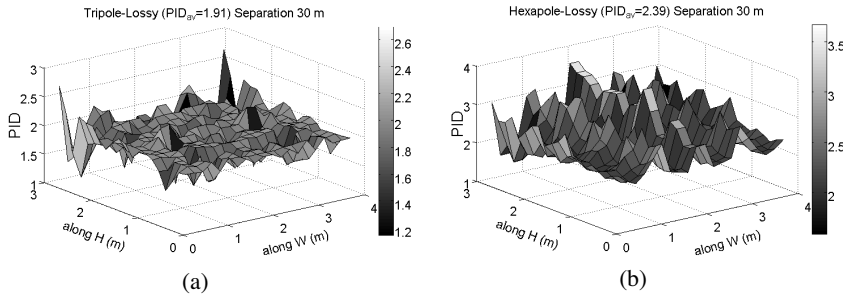


Figure 5. PID of multi-polarization MIMO system in a lossy-wall corridor. The receive grid is located at 30 m from the transmit along L . (a) Tripole. (b) Hexapole.

6. DISCUSSION AND CONCLUSION

In this paper we investigated the DOF of a collocated multi-polarization antenna system in 3 case studies. The first 2 canonical cases, the near-field free-space and PEC corridor, represent rigorously derived multipath scenarios which are very rich. Unlike the stochastic-based simulations, the full-rank 6 DOF was never achieved through a hexapole system in the deterministic simulations herein.

Also, by applying the plane-wave (or spherical ray) expansion on the field in all the 3 studied cases, we showed that the individual 2 DOF per plane-wave component is not automatically a bottle-neck to the system DOF. The incoming plane waves at different directions result in a higher DOF of the system, which is attributed to the FED (also known as far-field pattern diversity or functional orthogonality) in addition to the obvious vectorial (polarization) orthogonality by creating one more component in the resultant field. However, it can happen that the total plane wave contribution yields less than 2 DOF as observed in the case of the tripole system in the PEC waveguide.

A rich multipath environment is needed in order to achieve an acceptable DOF performance through a multipole system. We repeated the PEC corridor simulations with the transmit multipole situated at various locations and we obtained very close average PID values for the tripole and hexapole systems as those of Fig. 4. One can argue that the open-ended PEC waveguide has only a hemi-spherical angular spread of the rays and thus it is not as multipath-rich as the optimum PEC enclosure. In order to examine this argument, we made other simulations in a PEC corridor with only *one open end*. We placed the transmit multipole and the receive grid at $L = 50$ and $L = 75$ m, respectively and a PEC wall is located at $L = 100$ m. Therefore, we have full angular spread over the receive spherical solid angle and the modal solution is still fast convergent (evanescent modes are suppressed). We repeated the modal analysis including the multipole source image and we obtained very similar results to Fig. 4, including the average PID values. Again, the maximum PID value of 6 has never been attained.

We show a comparison between the PID normalized histogram of the PEC and lossy-wall ($LT \sim 0.01$) corridor multipole scenarios in Fig. 6. At each cross-section grid, we have 10^4 and 400 points for the PEC and lossy-wall corridor, respectively. The bin size for the normalized histogram, spanning the PID values from 1 to 6, is 0.1. In the multipath rich PEC case, the histogram in Fig. 6 indicates that by using a tripole system, there is some probability of achieving a PID close to the full-rank 3 DOF and also the PID can

happen to be less than 2. On the other hand, the hexapole system almost guarantees more than 3 DOF, however, it never attains the full 6 DOF. The transparent-wall corridor, lacking multipath richness, yielded significant PID reduction and the gap between the tripole and hexapole PID average value decreases.

We conclude by summarizing the concepts and findings of this paper *in the deterministic simulated scenarios*:

- There are 2 types of collocated orthogonality (vectorial and functional) responsible for the diversity when using electric and magnetic multipole systems. These 2 types are inter-twined due to the inevitable coupling between the electric and magnetic field components.
- In a sufficiently multipath-rich environment, a tripole system may provide very close PID to the maximum full-rank 3 DOF. A hexapole system does not automatically double the tripole dimensionality (6 DOF were never achieved), however, the hexapole system produces, in general, higher DOF (more than 3 DOF are almost guaranteed).
- The average PID is environment-dependent (electrical properties of boundaries) and seems to be independent of the deployment configuration (location of the transmit/receive multipole elements). The gap between the hexapole and tripole PID values decreases as the multipath richness decreases.

ACKNOWLEDGMENT

This work was supported by the Natural Sciences and Engineering Research Council of Canada (NSERC) and in part by Research In Motion (RIM).

APPENDIX A. POWER INDEPENDENT DIMENSIONALITY METRIC (PID)

We treat the dimensionality as a *power-independent* indicator of the available parallel sub-channels of the system. Accordingly, we did not use the MIMO capacity, which is a global power-dependent metric, to evaluate the DOF. Rather, we developed a power independent dimensionality (PID) metric [11], which depends only on the singular values of the channel matrix.

A MIMO channel matrix $\mathbf{H} \in \mathbb{C}^{N_R \times N_T}$, where (N_R, N_T) are the number of receive and transmit elements, respectively, can have up to $K = \min\{N_R, N_T\}$ parallel sub-channels. Consider another fictitious

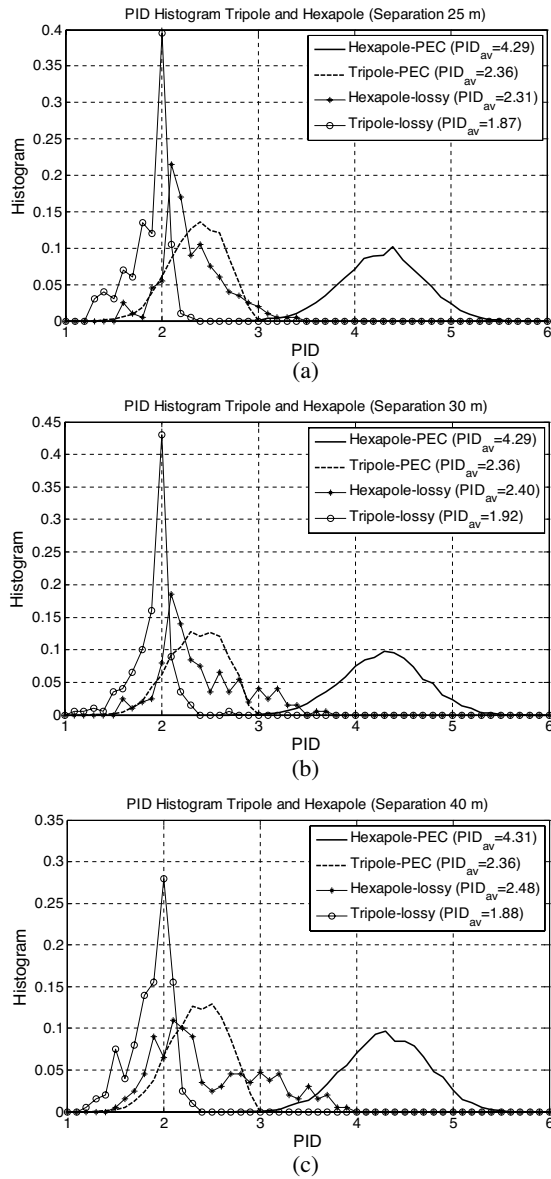


Figure 6. Normalized histogram of the tripole and hexapole systems PID in the PEC and lossy corridor. The receive grid is located at different separations along L , (a) 25 m, (b) 30 m, (c) 40 m.

channel $\mathbf{H}^{(\text{eq})}$, which has k equally contributing (out of K available) eigen channels whereas the remaining $(K - k)$ sub-channels have zero contribution. Obviously, $\mathbf{H}^{(\text{eq})}$ has k communication dimensions and its singular values are given by

$$\sigma_i^{(\text{eq})} = \begin{cases} \sigma_0 & i = 1, 2, \dots, k \\ 0 & i = k + 1, \dots, K \end{cases} \quad (\text{A1})$$

Our target is to estimate an effective value for k according to some equivalence criteria between \mathbf{H} and $\mathbf{H}^{(\text{eq})}$. Having 2 unknowns in (A1), σ_0 and k , we need 2 equivalence conditions. We choose to impose p - and q -Schatten-norm equivalence such that $\|\mathbf{H}\|_r \equiv \|\mathbf{H}^{(\text{eq})}\|_r$, where $r = \{p, q\}$. Accordingly,

$$k \triangleq \text{PID}_{pq} = \left[\left(\sum_{i=1}^K \sigma_i^q \right)^p / \left(\sum_{i=1}^K \sigma_i^p \right)^q \right]^{\frac{1}{p-q}} \quad p \neq q \in [1, \infty). \quad (\text{A2})$$

The values for p and q are arbitrary. For large values of p and q , the Schatten norm tends to the spectral norm (the largest singular value). Therefore, a choice of small p and q makes the PID more sensitive to the small singular values. In this work, we chose the values $p = 1$ and $q = 2$. Thus, the PID used throughout the paper is given by

$$\text{PID}_{12} = \left(\sum_{i=1}^K \sigma_i \right)^2 / \sum_{i=1}^K \sigma_i^2. \quad (\text{A3})$$

It can be shown that $1 \leq \text{PID}_{pq}(\mathbf{H}) \leq \text{rank}(\mathbf{H})$. Therefore, $\text{PID}_{pq}(\mathbf{H})$ can be viewed as a well-defined effective rank of the matrix \mathbf{H} .

REFERENCES

1. Andrews, M. R., P. Mitra, and R. De Carvalho, "Tripling the capacity of wireless communications using electromagnetic polarization," *Nature*, Vol. 409, 316–318, Jan. 2001.
2. Svantesson, T., M. A. Jensen, and J. W. Wallace, "Analysis of electromagnetic field polarizations in multiantenna systems," *IEEE Trans. Wireless Comm.*, Vol. 3, 641–646, Mar. 2004.
3. Piestun, R. and D. A. B. Miller, "Electromagnetic degrees of freedom of an optical system," *Optical Society of America*, Vol. 17, 892–902, May 2000.

4. Poon, A. S. Y., R. W. Brodersen, and D. N. C. Tse, "Degrees of freedom in multiple-antenna channels: A signal space approach," *IEEE Trans. Information Theory*, Vol. 51, 523–536, Feb. 2005.
5. Sarkar, T. K., M. Salazar-Palma, M. Wicks, and R. J. Bonneau, *Smart Antennas*, John Wiley & Sons, 2003.
6. Sarkar, T. K., S. Burintramart, N. Yilmazer, S. Hwang, Y. Zhang, A. De, and M. Salazar-Palma, "A discussion about some of the principles/practices of wireless communication under a Maxwellian framework," *IEEE Trans. Antennas Propagation*, Vol. 54, 3727–3745, Dec. 2006.
7. Harrington, R. F., *Time-harmonic Electromagnetic Fields*, McGraw-Hill, 1961.
8. Clemmow, P. C., *The Plane Wave Spectrum Representation of Electromagnetic Fields*, Oxford Pergamon Press, 1966.
9. Balanis, C., *Antenna Theory Analysis and Design*, John Wiley & Sons, 1997.
10. Elnaggar, M., S. Safavi-Naeini, and S. K. Chaudhuri, "Effect of oversimplifying the simulated indoor propagation on the deterministic MIMO capacity," *IEEE Canadian Conference on Electrical and Computer Engineering (CCECE 2004)*, Vol. 1, 219–222, Niagara Falls, ON, May 2004.
11. Elnaggar, M. S., S. Safavi-Naeini, and S. K. Chaudhuri, "A novel dimensionality metric for multi-antenna systems," *Proceedings of Asia-Pacific Microwave Conference (APMC2006)*, Yokohama, Japan, Dec. 2006.